Cellular and Molecular Life Sciences (2024) 81:2
https://doi.org/10.1007/s00018-023-05017-x

ORIGINAL ARTICLE

The senescent mesothelial matrix accentuates colonization by ovarian cancer cells

Bharat Vivan Thapa[1,2] · Mallar Banerjee[1] · Tilmann Glimm[3] · Deepak K. Saini[1,4] · Ramray Bhat[1,4]

Received: 6 June 2023 / Revised: 4 October 2023 / Accepted: 24 October 2023

Abstract

Ovarian cancer is amongst the most morbid of gynecological malignancies due to its diagnosis at an advanced stage, a transcoelomic mode of metastasis, and rapid transition to chemotherapeutic resistance. Like all other malignancies, the progression of ovarian cancer may be interpreted as an emergent outcome of the conflict between metastasizing cancer cells and the natural defense mounted by microenvironmental barriers to such migration. Here, we asked whether senescence in coelom-lining mesothelia, brought about by drug exposure, affects their interaction with disseminated ovarian cancer cells. We observed that cancer cells adhered faster on senescent human and murine mesothelial monolayers than on non-senescent controls. Time-lapse epifluorescence microscopy showed that mesothelial cells were cleared by a host of cancer cells that surrounded the former, even under sub-confluent conditions. A multiscale computational model predicted that such colocalized mesothelial clearance under sub-confluence requires greater adhesion between cancer cells and senescent mesothelia. Consistent with the prediction, we observed that senescent mesothelia expressed an extracellular matrix with higher levels of fibronectin, laminins and hyaluronan than non-senescent controls. On senescent matrix, cancer cells adhered more efficiently, spread better, and moved faster and persistently, aiding the spread of cancer. Inhibition assays using RGD cyclopeptides suggested the adhesion was predominantly contributed by fibronectin and laminin. These findings led us to propose that the senescence-associated matrisomal phenotype of peritoneal barriers enhances the colonization of invading ovarian cancer cells contributing to the metastatic burden associated with the disease.

Keywords Chemotherapy · Extracellular matrix · Mesothelia · Multiscale modeling · Ovarian cancer · Senescence

Introduction

The high morbidity associated with epithelial ovarian cancer (EOC) is due to its ability to rapidly metastasize and colonize the visceral peritoneum. Transformed cells at the primary site are shed into the peritoneal cavity via the movement of peritoneal fluid. Ovarian cancer cells adhere to the lining of the peritonea [1, 2], retract mesothelial cells [3], and actively degrade the underlying and exposed extracellular matrix (ECM) by expressing proteolytic enzymes such as matrix metalloproteinases (MMPs) [2]. Management of EOC involves surgical cytoreduction with chemotherapy provided before or/and after surgery [4]. Cytotoxic therapeutics commonly employed in EOC are carboplatin and doxorubicin, which bind to and alkylate DNA, and paclitaxel, which binds to tubulin and prevents karyokinesis. Treatment with these agents inhibits cell division and ultimately leads to cell death. However, exposure to such drugs may also induce a cytostatic (as opposed to cytotoxic) state in both cancer and primary cells, also known as senescence, wherein the cells are metabolically active but growth-arrested. Therapy-induced senescence (TIS) has been proposed to suppress tumor cell proliferation [5]. On the other hand, it has also been shown to potentiate tumor heterogeneity, resistance [6], and relapse [7]. For instance, TIS in ovarian cancer cells

✉ Deepak K. Saini
deepaksaini@iisc.ac.in

✉ Ramray Bhat
ramray@iisc.ac.in

[1] Department of Developmental Biology and Genetics, Indian Institute of Science, Bangalore 560012, India

[2] Undergraduate Program, Indian Institute of Science, Bangalore 560012, India

[3] Department of Mathematics, Western Washington University, Bellingham, WA 98229, USA

[4] Department of Bioengineering, Indian Institute of Science, Bangalore 560012, India

Published online: 03 December 2023

leads to their transient dormancy, which can be reversed to re-initiate proliferation [8, 9]. TIS-associated cytokine secretion (as part of the broader phenomenon of senescence-associated secretory phenotype or SASP) may accentuate infiltration by tumor-associated macrophages (TAMs) in primary tumors leading to greater invasion and metastasis [10–12].

Exposure to therapeutic drugs can affect not just the transformed cell niche within a tumor but also the untransformed cellular microenvironment in ways that engender disease progression. Stromal constituents such as endothelial cells and bone marrow-derived cells signal in response to chemotherapeutic exposure to accentuate metastasis [13–16]. In this context, it is pertinent to study whether senescence in stromal constituents due to drug exposure contributes to cancer cell invasion. Indeed, the accumulation of senescent/aged mesothelia, the cells lining the peritoneal cavity, has been shown to aid ovarian cancer metastasis [17].

In this study, we sought to ask whether chemotherapeutic drugs can drive mesothelial cells to senescence with an unintended potentiation of cancer progression. Using a human-murine hybrid ex vivo system, human mesothelial-cancer coculture system and a Cellular Potts Model (CPM)-based multiscale framework, we found that the senescent mesothelia secrete a unique matrisome that provides a habitable niche for metastasizing cancer cells. A comprehensive understanding of how such a 'senescence-associated matrisomal phenotype' leads to higher invasion by ovarian cancer will help design novel therapeutics for the management of metastasis.

Results

Senescent mesothelial monolayers potentiate adhesion of ovarian cancer cells

Parietal peritoneal tissue was dissected from 4 to 6 week Balb/c female mice and cultivated ex vivo as described earlier [18]. Senescence was induced in the explants using 100 nM doxorubicin. Mesothelial cells were harvested from control and senescent murine peritonea and senescence was confirmed by morphological examination (Figure S1A). Control and senescent explants were cultivated with a suspension of GFP-expressing SKOV-3 cells and the adhesion of the latter assessed (Fig. 1A). SKOV-3 cells were observed to attach faster to the senescent murine peritoneum than untreated controls (Fig. 1Bi-ii; statistical significance shown in Fig. 1Biii).

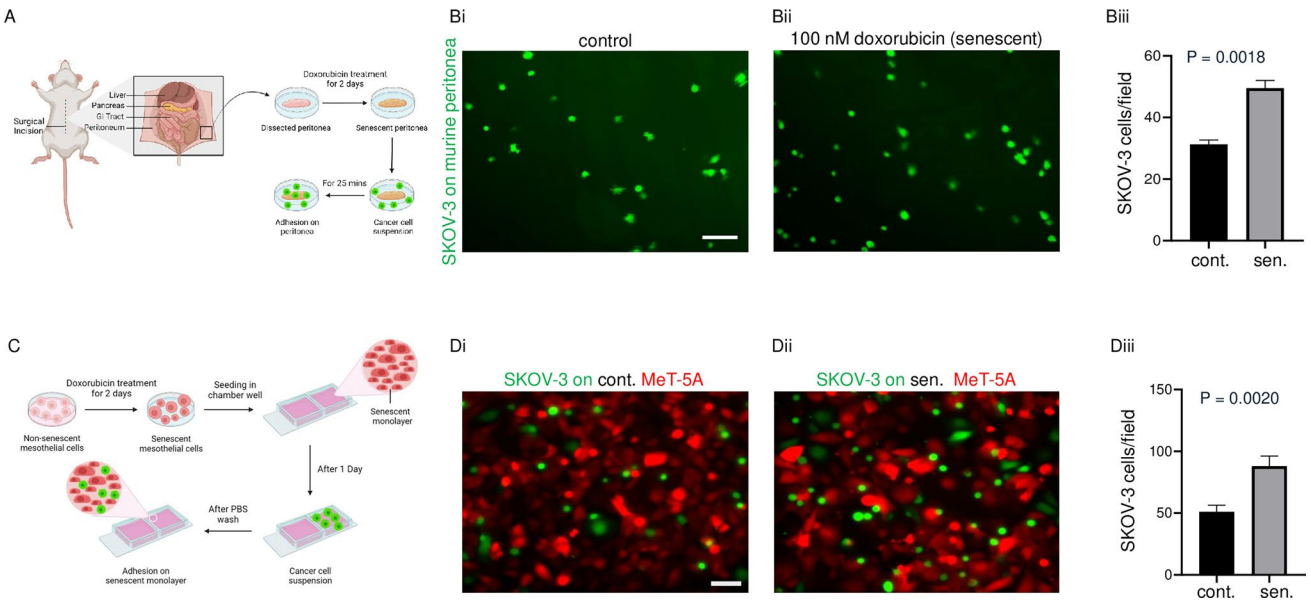

Fig. 1 Effect of a senescent mesothelial microenvironment on the adhesion of ovarian cancer cells (**A**) Schematic depiction of the adhesion assay performed on murine peritonea that were rendered senescent using 100 nM doxorubicin, cultivated ex-vivo in the presence of ovarian cancer cell suspension. **B** Representative fluorescence micrographs showing the adhesion of GFP-expressing SKOV-3 cells on control murine peritonea (i), senescent murine peritonea (ii), and bar graph showing the number of adhered SKOV-3 cells per field for control and senescent murine peritonea (iii). **C** Schematic depiction of the adhesion assay performed on RFP-expressing control and doxorubicin-induced senescent MeT-5A monolayers cultivated in the presence of GFP-expressing ovarian cancer cells. **D** Representative fluorescence micrographs showing the adhesion of GFP-expressing SKOV-3 cells on control MeT-5A monolayer (i), senescent MeT-5A monolayer (ii), and a bar graph showing the number of SKOV-3 cells per field for control and senescent MeT-5A monolayers (iii). The fields are at 10× magnification with a scale bar of 100 µm. The experiments were performed in triplicates. The data are presented as mean ± SEM and significance is obtained using an unpaired parametric t-test with Welch's correction

We did not observe any notable difference in acellular spaces between control and senescent mesothelial monolayers prior to the adhesion of cancer cells, which suggested that clearance rather than available adherable space could play a role in a greater cancer cell occupancy within senescent cell populations.

To confirm that the clearance of senescent MeT-5A monolayers is indeed caused by SKOV-3 cells, a senescent monolayer without SKOV-3 cells was also imaged for 72 h (Figure S4A; see also video S3). We observed a significant reduction in the area occupied by senescent MeT-5A monolayers in the presence of SKOV-3 cells compared to SKOV-3-less controls (Fig. 2Di and Figure S4B). To confirm the ability of ovarian cancer cells to clear, and proliferate amidst, senescent mesothelia, GFP-expressing OVCAR-3 cells were cultivated with senescent and control MeT-5A monolayers for 60 h (Figure S5A and S5B). We observed higher proliferation of OVCAR-3 cells within senescent MeT-5A monolayers (Figure S5Ci-ii) and a significant reduction in the area occupied by senescent MeT-5A monolayers compared with control MeT-5A monolayers (Figure S5Di-ii). We also observed a substantial decrease in the area occupied by senescent MeT-5A monolayers cultured with OVCAR-3 cancer cells compared with senescent MeT-5A monolayers where with OVCAR-3 cells were not added (Figure S5E-F and Di).

Multiple cancer cells surround and clear senescent mesothelia independent of confluence

Extrusion of cells within populations is well known across developmental and oncological contexts and is often driven through cell-density dependent mechanisms [19, 20]. We asked if the clearance of mesothelia was achieved by cancer cells only when both were part of a jammed confluent population. To answer this question, we examined our epifluorescence time-lapses and observed senescent cell extrusions by SKOV-3 cells even in sub-confluent conditions (Fig. 3A). We found that the total number of extrusions in senescent MeT-5A monolayers with SKOV-3 cells was significantly higher than the total number of extrusions in control MeT-5A monolayers with SKOV-3 cells and senescent MeT-5A monolayers without SKOV-3 cells (Fig. 3B). Moreover, we observed that a significant number of extruded senescent MeT-5A were surrounded and impacted by more than one SKOV-3 cell before their clearance (Fig. 3C). To our surprise, we also observed that senescent cells distant from SKOV-3 cells showed a lower frequency for extrusion (similar to non-senescent cells in controls distant from SKOV-3 cells. This suggested that the extrusion of senescent mesothelial cells was strongly correlated with their proximity with ovarian cancer cells.

To further characterize cellular neighborhoods within coculture monolayers, we determined the total number and type of neighbors for senescent and non-senescent mesothelia within cocultures. Due to their larger surface area, the number of neighbors for senescent cells is naturally higher (~4–5 cells) than for non-senescent cells (~2–3 cells). Nevertheless, the proportion of neighboring cells being cancer cells was found to be significantly higher for senescent mesothelia than their counterpart non-senescent cells in the same fields (Fig. 3D).

Our observation that cancer cells can clear mesothelia independent of cell crowding effects suggested that confluence dependent cell extrusion may not be operative here. This surmise was reinforced by our observation of a closer localization of cancer cells to senescent mesothelia. To shed light on the intercellular interactions that allow confluence-agnostic senescent cell shedding, we employed a multiscale virtual tissue simulation approach using the Cellular Potts Model (CPM)-based computational framework Compucell3D. A monolayer consisting of senescent, non-senescent, and cancer cells was simulated initially, incorporating differences in their cell proliferation rates and relative cell size. The simulation period in Monte-Carlo steps (MCS) was calibrated with experiments by comparing the growth of cancer cells in the experiments to the growth rate of cancer cells in simulations. The size and number of each cell type was quantified based on their initial starting conditions in experiments. Our first model (Fig. 4Bi; video S4) incorporated no other interactive rule. It was, therefore, not surprising that the first model resulted in a confluent monolayer without any colocalization of cancer cells and senescent cells and without any clearance of the latter. Based on our observations in Fig. 3A, we incorporated an additional rule (Model 2, Fig. 4Bii; video S5), wherein clearance of senescent cells could occur if they share $>=55\%$ of their perimeter with cancer cells. This did result in the extrusion of senescent cells, but only after cancer cells had proliferated enough to create a confluent cocultured monolayer. Therefore, clearance occurred much after confluence had been reached. This led us to hypothesize that an effective attractive force may exist between senescent and cancer cells, driving them to localize close to each other (consistent with our experimental observations of their proximity). Solely implementing such an attractive force (through decreasing the contact energy of adhesion between the senescent and cancer cells; $CE_{new}=15$, while $CE_{old}=30$) was insufficient for mesothelial clearance (Model 3, Fig. 4Biii; video S6). However, the simultaneous implementation of adhesive attraction between senescent and cancer cells and the rule for extrusion (Model 4, Fig. 4Biv; video S7) brought about clearance even when the monolayers were sub-confluent, similar to what we observed in experiments (as shown in Fig. 4C, D). We next asked whether senescent cells secreted any chemoattractants

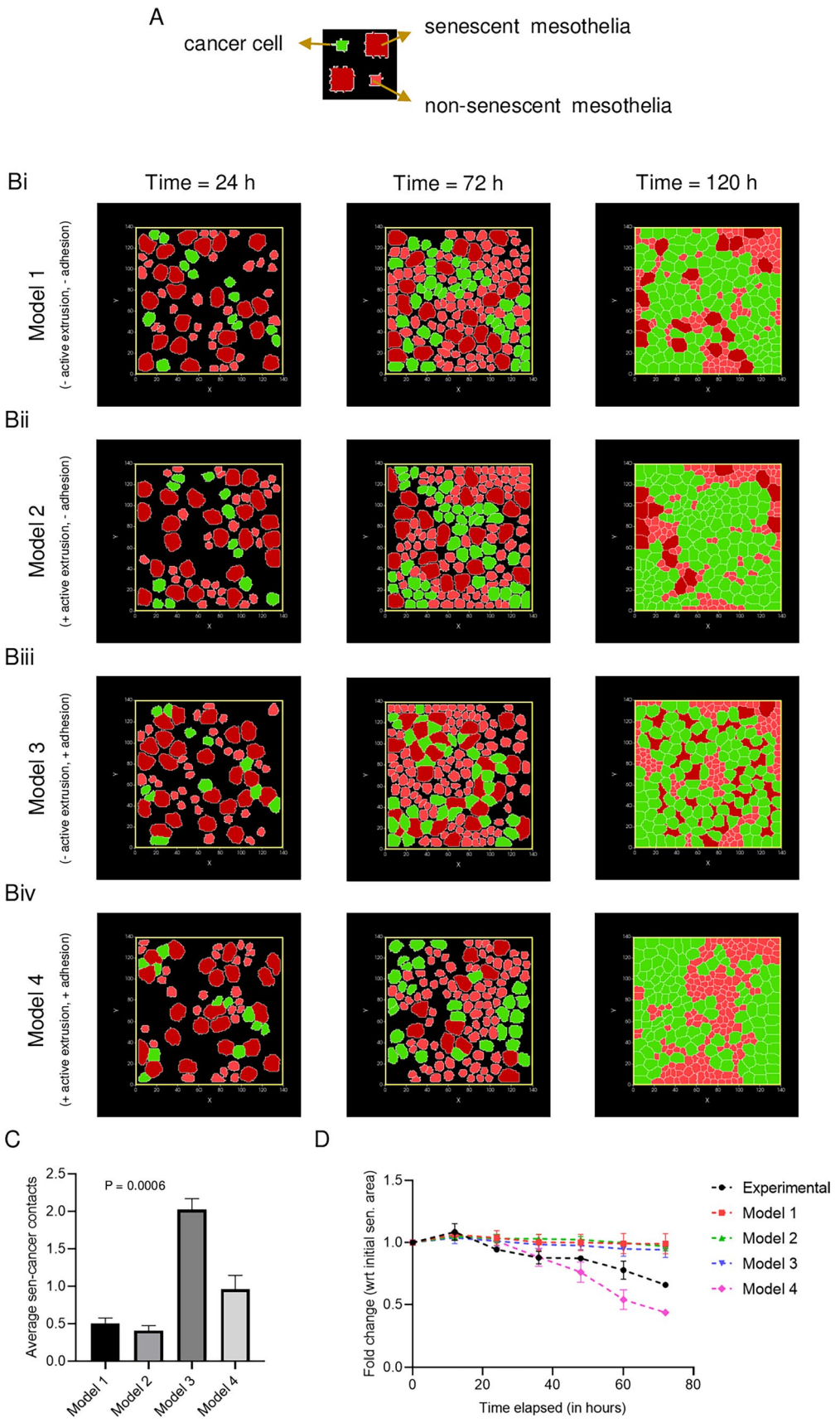
A
cancer cell
senescent mesothelia
non-senescent mesothelia
Bi
Time = 24 h
Time = 72 h
Time = 120 h
Model 1
(- active extrusion, - adhesion)
Bii
Model 2
(+ active extrusion, - adhesion)
Biii
Model 3
(- active extrusion, + adhesion)
Biv
Model 4
(+ active extrusion, + adhesion)
C
P = 0.0006
Average sen-cancer contacts
Model 1
Model 2
Model 3
Model 4
D
Fold change (wrt initial sen. area)
Time elapsed (in hours)
Experimental
Model 1
Model 2
Model 3
Model 4

199 media (HiMedia; AL014A) along with 10% fetal bovine serum (Gibco; 10,270) were used for conditioned media growth assay with SKOV-3 cancer cells.

Senescent and non-senescent matrix preparation

Senescent and non-senescent MeT-5A cells were seeded at high confluency on chamber wells with coverslip bottoms. The cells were allowed to adhere and lay down the extracellular matrix for the next 36 h. The confluent MeT-5A monolayers were then washed with 1 × PBS twice and decellularized using a 20 mM solution of NH_4OH in Milli-Q water for 7–10 min [49]. The cellular debris was gently removed by giving 2–3 washes with Milli-Q water. The extracted extracellular matrices laid on the chamber wells were used for adhesion assays.

Adhesion assay with RGD peptide

The SKOV-3 cells (5000 in number) suspended in Mcoy's 5A media (HiMedia; AL057A) along with 10% fetal bovine serum (Gibco; 10,270) were added to the decellularized senescent and non-senescent matrices and allowed to adhere on the matrix for 25 min. For adhesion assay with RGD peptide, the media also had cyclic RGD peptide (Sigma; G1269-1MG) at 10 and 20 µg/mL concentrations. After incubation, the wells were washed with 1 × PBS twice and immediately imaged by using an Olympus IX83 inverted epifluorescence microscope at 10 × magnification. The images were analyzed and the number of cells adhered to the matrices was counted using the "analyze particles" feature in ImageJ. The attached cells were also time-lapsed for 24 h using a Tokai Hit stage-top incubator with image acquisition through an Orca Flash LT plus camera (Hamamatsu) on an Olympus IX73 microscope. The data were analyzed using a manual tracking plugin in FIJI and Ibidi's chemotaxis and migration tool to see differences in displacement and velocity of SKOV-3 cells on senescent and non-senescent matrices (can be seen in videos S8 and S9).

Compucell 3D model for the clearance of senescent mesothelia

Compucell3D (CC3D) is based on the Cellular Potts Model (CPM), also known as the Glazier-Graner-Hogeweg (GGH) model. It has been utilized extensively for computational models of the collective behavior of cellular structures. The CPM is a lattice-based discrete model in which spatiotemporal development is simulated via an energy minimizing procedure [34, 50]. Each cell consists of a collection of lattice sites (pixels). Each configuration is associated with an effective energy, or Hamiltonian (H), which is calculated based on properties such as volume, surface area, contact energies, or external properties. Time evolution is simulated via Monte Carlo Steps (MCS) that involve random changes of lattice site occupations and the changes that decrease the energy are more likely than those that increase it. The Hamiltonian of the system is formulated as:

$$H = \sum_{i,jneighbors} J\left(\tau\left(\sigma_i\right),\left(\sigma_j\right)\right)\left(1-\delta\left(\sigma_i,\sigma_j\right)\right) + \lambda \sum_{\sigma_i} \left(v\left(\sigma_i\right) - V(\sigma_i)\right)^2$$

where i, j are lattice sites, σ_i is the cell at site i, $\tau(\sigma)$ is the cell type of cell σ, J is the coefficient determining the adhesion between two cells of types $\tau(\sigma)$, $\tau(\sigma\prime)$, δ is the Kronecker delta, v(σ) is the volume of cell σ, V(σ) is the target volume, and λ is a Lagrange multiplier determining the strength of the volume constraint. We utilized a simple two-dimensional model 140*140*1 using a square pixel lattice to find and understand the effect of factors sufficient to bring a considerable decline in the senescent mesothelia area as observed in the mesothelial clearance experiments that were recorded using time-lapse epifluorescence videography. The simulation time was set to 8000 MCS as per the corresponding normalized length of the experimental time-lapse videos. The lattice is composed of the medium, senescent cells (SEN), non-senescent cells (NON_SEN), ovarian cancer cells (CANCER), and a frozen wall that mimics a closed system such as enclosed peritoneal cavity (shown in figure S12). This simple model has four variations with the contact energies between cancer and senescent cells to be either 15 (greater adhesion) or 30 (same as other contact energy combinations) and activation or deactivation of the active extrusion rule (shown in figure S13). The other important parameters used in the model and their input values are available at Table S2. To compare the simulation time to the timescale of senescent mesothelial clearance by ovarian cancer cells, a calibration was performed. The division time of ovarian cancer cells in experiments (SKOV-3 cells) was 18 h and the division time of ovarian cancer cells in simulations was 750 MCS. This factor was used to calibrate the simulations time to real-time and the comparison between the computational model and senescent mesothelial clearance experiments was made.

Statistical analysis

The experiments were repeated at least three times and unpaired parametric t-test with Welch's correction were used for statistical testing unless otherwise stated in the figure legends. The graphs were plotted using GraphPad Prism 8.0.2 and p-values < 0.05 was considered statistically significant.

Supplementary Information The online version contains supplementary material available at https://doi.org/10.1007/s00018-023-05017-x.

Acknowledgements The authors would like to thank Abraham Binoy Mathew for technical help with senescence induction.

S11

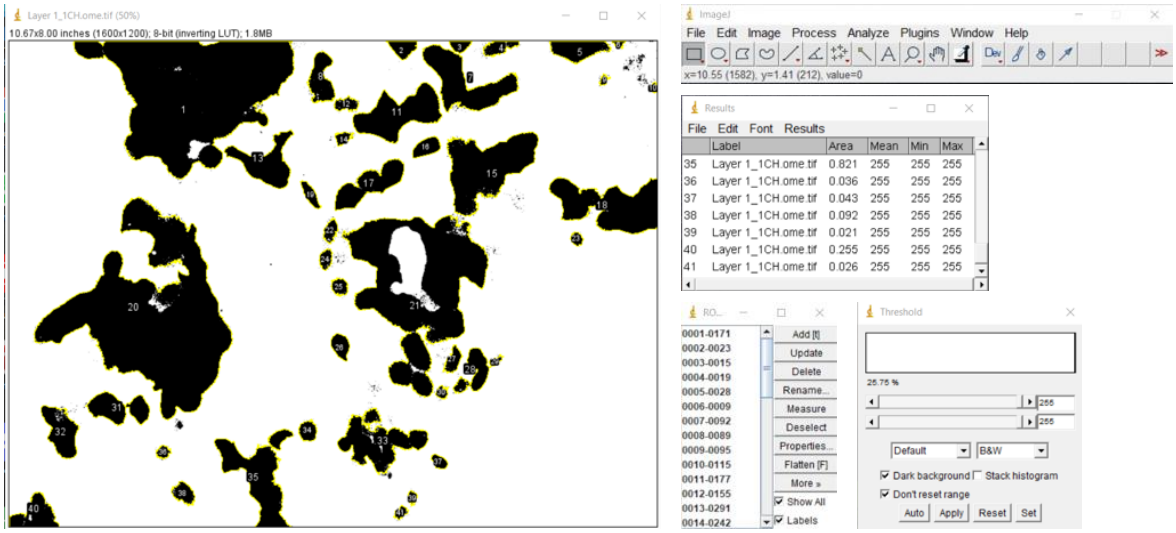

Screenshot showing the analysis performed on images collected from mesothelial clearance assay to calculate the area occupied by MeT-5A and SKOV-3/OVCAR-3 cells in the same field. The highest value of the threshold with a neat background was chosen for generating the mask. The area of cells in the field was measured by summing up the individual particle area and is calculated under the 'Analyze particles' options with size limit = 0.01-Infinity.

S12

Cell Type Id	Color	Name
0		Medium
1		SEN
2		NON_SEN
3		CANCER
4		WALL

Property	Value
Revision	2
Version	4.3.0
Metadata	Metadata
Potts	Potts
Plugin	CellType
Plugin	Volume
Plugin	Surface
Plugin	ExternalPotential
Plugin	CenterOfMass
Plugin	NeighborTracker
Plugin	Contact
Plugin	Chemotaxis
Plugin	Secretion
Steppable	DiffusionSolverFE
Steppable	UniformInitializer

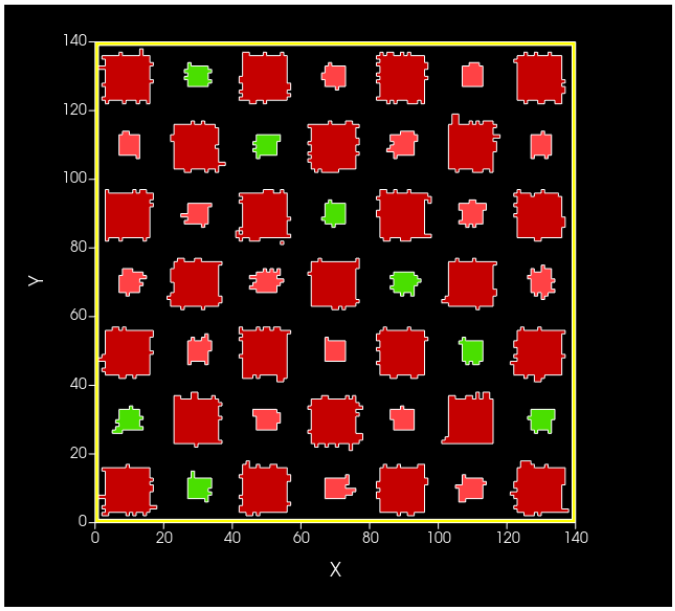

A snapshot of the initial layout of the different cells on the lattice – The picture depicts the initial layout of senescent, non-senescent, and cancer cells in a two-dimensional setup and the incorporated plugins. The relative sizes and the proliferation rates of the three cell types were calibrated from the experiments.

```
common_area_frac = 0.55
for cell in self.cell_list_by_type(self.SEN):
    Avol_SEN += cell.volume/L_SEN
    cancer_common_area = 0
    for neighbor, common_surface_area in self.get_cell_neighbor_data_list(cell):
        if neighbor and neighbor.type == self.CANCER:
            cancer_common_area += common_surface_area
             Average_cancer_neighbours += 1

    # Active clearance rule is impleted in the next three line
    if cancer_common_area/cell.surface > common_area_frac:
        cell.targetVolume = 0
        cell.lambdaVolume = 10000
```

A snapshot of the active clearance code from Twedit++5 – The code shows the implementation of the killing of senescent cells if more than 55% of their perimeter is shared with ovarian cancer cells.

Gene name	Forward primer (5'→3')	Reverse primer (5'→3')
GAPDH	GGAGCGAGATCCCTCCAAAA	GGCTGTTGTCATACTTCTCATGG
p21	GGAAGACCATGTGGACCTGT	TAGGGCTTCCTCTTGGAGAA
Gal-9	CCTACCTGAGTCCAGCTGTC	GAGGGTTGAAGTGGAAGGCA
LamB3	GCAGCCTCACAACTACTACAG	CCAGGTCTTACCGAAGTCTGA
Col6A1	ACAGTGACGAGGTGGAGATCA	GATAGCGCAGTCGGTGTAGG
FN1	CAAGCCAGATGTCAGAAGC	GGATGGTGCATCAATGGCA
LamA3	CACCGGGATATTTCGGAATC	AGCTGTCGCAATCATCACATT
Col18A1	CAGTGGACACACTTAGCCCTC	GCGGCATTCTCTGGAACTCC
FBLN1	AGAGCTGCGAGTACAGCCT	CGACATCCAAATCTCCGGTCT
FBLN-1C	TGACTGGCATCCACAACTGC	GCTTGGAGCACTCCCGATTCT
FBLN-1D	TGCCTACCTTCCGCGAGTTC	GCCGTCCATGTAACGCTTGA
Gal-1	TCAAACCTGGAGAGTGCCTT	CACACCTCTGCAACACTTCC
Gal-3	ATGGCAGACAATTTTTCGCTCC	GCCTGTCCAGGATAAGCCC

Table 1 – RT PCR primer sequence information for the gene expression studies in non-senescent and senescent MeT-5A monolayers

```
<CompuCell3D Revision="2" Version="4.3.0">

   <Metadata>

      <!-- Basic properties simulation -->
      <NumberOfProcessors>4</NumberOfProcessors>
   </Metadata>

   <Potts>

      <!-- Basic properties of CPM (GGH) algorithm -->
      <!-- Basic properties of CPM (GGH) algorithm -->
      <Dimensions x="140" y="140" z="1"/>
      <Steps>100000</Steps>
      <Temperature>20.0</Temperature>
      <NeighborOrder>1</NeighborOrder>
      <!-- <Boundary_x>Periodic</Boundary_x> -->
      <!-- <Boundary_y>Periodic</Boundary_y> -->
   </Potts>

   <Plugin Name="CellType">

      <!-- Listing all cell types in the simulation -->
      <CellType TypeId="0" TypeName="Medium"/>
      <CellType TypeId="1" TypeName="SEN"/>
      <CellType TypeId="2" TypeName="NON_SEN"/>
      <CellType TypeId="3" TypeName="CANCER"/>
      <CellType Freeze="" TypeId="4" TypeName="WALL"/>
   </Plugin>


   <Plugin Name="Contact">
      <!-- Specification of adhesion energies -->
      <Energy Type1="Medium" Type2="Medium">10.0</Energy>
      <Energy Type1="Medium" Type2="SEN">10.0</Energy>
      <Energy Type1="Medium" Type2="NON_SEN">10.0</Energy>
      <Energy Type1="Medium" Type2="CANCER">10.0</Energy>
      <Energy Type1="SEN" Type2="SEN">30.0</Energy>
      <Energy Type1="SEN" Type2="NON_SEN">30.0</Energy>
      <Energy Type1="SEN" Type2="CANCER">30.0</Energy>
      <Energy Type1="NON_SEN" Type2="NON_SEN">30.0</Energy>
      <Energy Type1="NON_SEN" Type2="CANCER">30.0</Energy>
      <Energy Type1="CANCER" Type2="CANCER">30.0</Energy>
      <Energy Type1="WALL" Type2="SEN">50.0</Energy>
      <Energy Type1="WALL" Type2="NON_SEN">50.0</Energy>
      <Energy Type1="WALL" Type2="CANCER">50.0</Energy>

      <NeighborOrder>4</NeighborOrder>
   </Plugin>

   <Plugin Name="Chemotaxis">

      <!-- You may repeat ChemicalField element for each chemical field declared in the PDE
      solvers -->
      <!-- Specification of chemotaxis properties of select cell types. -->
      <ChemicalField Name="CHEMOKINE">
        <ChemotaxisByType ChemotactTowards="NON_SEN" Lambda="0" Type="CANCER"/>
      </ChemicalField>
      <ChemicalField Name="CHEMOKINE">
        <ChemotaxisByType ChemotactTowards="CANCER" Lambda="0" Type="CANCER"/>
      </ChemicalField>
```

```
      <ChemicalField Name="CHEMOKINE">
        <ChemotaxisByType ChemotactTowards="Medium" Lambda="0" Type="CANCER"/>
      </ChemicalField>
   </Plugin>


   <Steppable Type="DiffusionSolverFE">

      <!-- Specification of PDE solvers -->
      <DiffusionField Name="CHEMOKINE">
         <DiffusionData>
            <FieldName>CHEMOKINE</FieldName>
            <GlobalDiffusionConstant>0.1</GlobalDiffusionConstant>
            <GlobalDecayConstant>0.0002</GlobalDecayConstant>
         </DiffusionData>
         <BoundaryConditions>
            <Plane Axis="X">
               <ConstantDerivative PlanePosition="Min" Value="0.0"/>
               <ConstantDerivative PlanePosition="Max" Value="0.0"/>
            </Plane>
            <Plane Axis="Y">
               <ConstantDerivative PlanePosition="Min" Value="0.0"/>
               <ConstantDerivative PlanePosition="Max" Value="0.0"/>
            </Plane>
         </BoundaryConditions>
      </DiffusionField>
   </Steppable>

   <Steppable Type="UniformInitializer">
   </Steppable>
</CompuCell3D>
```